metals

MDPI

Article

New Creep Crack Growth Prediction Model for the Life Assessment of Stainless-Steel Material Using Computational Modeling

Mohsin Sattar [1], Abdul Rahim Othman [1,*], Muhammad Firdaus Othman [2], Hafiz T. Ali [3] and Muhammad Kashif Khan [4]

[1] Department of Mechanical Engineering, Universiti Teknologi PETRONAS, Bandar Seri Iskandar 32610, Malaysia; mohsin.sattar@utp.edu.my
[2] Group Technical Solutions, Level 15 Tower 3, Kuala Lumpur Convention Centre, Kuala Lumpur 50088, Malaysia; mfirdaus.othman@petronas.com
[3] Department of Mechanical Engineering, College of Engineering, Taif University, Taif 21944, Saudi Arabia; htali@tu.edu.sa
[4] Centre for Manufacturing and Materials, Coventry University, Priory Street, Coventry CV1 5FB, UK; ac1291@coventry.ac.uk
* Correspondence: rahim.othman@utp.edu.my

Abstract: The limitations of the established and existing creep failure models have inspired the development of a new creep prediction model. Models like Norton–Bailey and Omega are unable to model the tertiary creep curve for engineering materials. Kachanov–Rabotnov, Theta Projection, and Sine hyperbolic models rely on specific material properties for accurate damage predictions. In order to overcome these weaknesses, a new creep model combining the Norton–Bailey and Kachanov–Rabotnov models has been further devised for the creep life prediction of metallic materials. The model combination helps in covering the limitations of one model over another and to benefit from each other's strengths. A technique of user subroutine scripting was adapted to implement the new creep model in finite element (FE) software of ABAQUS, manufactured by Dassault Systemes, version 2020. The new model was tested on an FE dog bone stainless steel 304 specimen; the analysis showed excellent agreement with the experimental creep deformation data at 600 °C to 700 °C. The creep strain rate curves obtained by the method of user subroutine scripting were found to be 90.69% accurate to the 1000 h experimental creep strain rate curve. Similarly, while comparing with the 336 h experimental creep test, the new model accuracy was found to be 92.66% for the creep strain rate curve. The new model's precision was 91.56% when compared with the Omega and Norton–Bailey models for creep strain rate for the same conditions. The quantitative accuracy of the new creep model is better as compared to the existing creep models and can be an improved source of alternatives to existing creep models for the deformation predictions.

Keywords: creep damage; stress rupture; Norton–Bailey model; Kachanov–Rabotnov model; plastic deformation

Citation: Sattar, M.; Othman, A.R.; Othman, M.F.; Ali, H.T.; Khan, M.K. New Creep Crack Growth Prediction Model for the Life Assessment of Stainless-Steel Material Using Computational Modeling. *Metals* **2023**, *13*, 1854. https://doi.org/10.3390/met13111854

Academic Editors: George A. Pantazopoulos and Sergei Alexandrov

Received: 28 September 2023
Revised: 27 October 2023
Accepted: 28 October 2023
Published: 6 November 2023

1. Introduction

Creep deformation is a time-dependent process that occurs under constant stress at elevated temperatures and can result in material failure if left unchecked. The phenomena labeled as 'cold flow' usually occurs when the material's temperature is greater than 40% of its melting temperature (T_m) [1]. Creep failure is critical because, at elevated temperatures, the strength of the material becomes dependent on strain rate and time [2]. Creep can cause microstructure damage, such as the creation of voids at grain boundaries, resulting in grain boundaries sliding and leading to material collapse [3]. Dislocation-climb and stress-induced vacancy flow at higher temperatures are two diffusion-controlled mechanisms

that cause creep in metals [4]. The movement of dislocations controls the creep intensity and the amount of damage inflicted on the material [5]. The creep life of components is determined by using various creep prediction models in finite element software because creep experiment testing is tedious, complex, and not cost-efficient [6]. Although creep tests are absolutely necessary for any type of material and condition, with the help of creep prediction modeling and computational finite element analysis, the number of tests can be reduced considerably. The creep tests take extensive time to complete, and there is difficulty in testing the specimen in the laboratory at elevated temperatures. Even slight variations in the temperature and loadings can disrupt the whole creep testing effort and the results [7].

Several empirical and theoretical creep life prediction models were developed over the years that claimed to accurately describe and predict the creep deformation behavior of materials [8]. These models used some assumptions in the analysis, which caused limitations in accurately predicting the creep deformation and remaining life of engineering components [9]. The current state-of-the-art of creep deformation prediction is mostly based on five established models, which include Norton–Bailey, Kachanov–Rabotnov, Omega, Theta projection, and Sine hyperbolic models [10]. Each model has its own limitations and is found to work only in specific environments and loading conditions [11].

The Norton–Bailey model can be found in the commercial finite element software package ABAQUS, built by Dassault Systemes, version 2020 [12], and is considered the benchmark model for creep damage models [13]. The model uses the power law to describe the creep strain rate with time to failure using a material constant as the power exponent [14]. The model does not take into account the primary and tertiary creep regions and only uses strain rate in the secondary creep domain for creep deformation [15]. The material constants used in this model vary with temperature, and the creep deformation prediction at higher temperatures was found to have variations with experimental results [12]. The Omega creep model has been included in ASME FFS-1 API/579-1 standards [16], initially adapted by the American Petroleum Institute, Materials Properties Council (MPC) [17]. The fracture strain in the MPC Omega model is difficult to estimate for the equipment under service due to limited temperature-dependent materials data at elevated temperatures. The model also does not provide any means for the indication of prior and ongoing damage in the material where the crack initiates and probably grows [18]. Omega method has shown relatively better accuracy in predicting material's rupture time at lower temperatures, as the margin of error is small between actual and predicted rupture time as compared to higher temperature conditions. The model requires curve fitting for extrapolation, as it is unable to model the exponential creep data, and the constants in the model equation are dependent on specific material properties.

On the other hand, the Kachanov–Rabotnov (KR) model uses coupled creep damage constitutive equations [19] and has shown more promising results. The damage evolution parameter in the equation is responsible for modeling the tertiary creep. The drawback is that it involves a large number of material constants and does not consider the primary creep in life prediction [20]. The model emulates continuum creep damage and discontinuous plastic damage at rupture using a continuous function, resulting in complexities in integration in FE analysis [21]. The Theta Projection (TP) method uses four material constants. The magnitude, curvature, and formation of the primary creep regime are controlled by the first two constants, whereas the tertiary creep is controlled by the other two constants. The model uses large empirical data to accurately define a single curve for accurate modeling. The process requires several curves at multiple conditions with intensive extrapolation within the same family of curves to precisely curve fit the data [22]. Recently, the Sine-Hyperbolic (SH) model has been successfully developed to overcome the limitations of other models, but the model is conservative in approach as it relies on specific material properties. The model yields good agreement with experimental results compared to other models [23].

Therefore, there is a need to develop a more robust and reliable creep model that can capture the complex creep deformation behavior of materials and predict the accurate

remaining life of engineering materials and components [24]. In this paper, a new creep prediction model based on the creep power laws was proposed [25]. The model was developed using the time-temperature superposition principle by integrating Norton–Bailey, and Kachanov–Rabotnov models using the continuum damage mechanics approach to cover the limitations of one model over another [26]. The model was employed in the FE package ABAQUS using a user subroutine scripting method [27]. The developed model was tested on FE dog bone stainless steel 304 specimens to predict the creep deformation stages with higher accuracy than other existing models when compared with the experimental data [28]. It was concluded that the numerical approach to implementing the model provides more freedom in application for the creep life prediction of engineering components with complex geometries [29]. The newly developed creep model has an edge over existing models due to the less reliance on specific material properties of the material while predicting creep damage [30].

The work undertaken in this manuscript is relevant to the field of fracture mechanics because of the uncertainty in predicting creep crack growth and creep deformation behavior of the material when exposed to extreme service conditions and to avoid catastrophic equipment failures [31]. A number of prediction models were proposed in the past, but they have their limitations [32]. The purpose of the research is to propose a new creep prediction model to cover the limitations of previous models for stainless steel material [33]. The model will give FE practitioners a reliable option to select and implement the new model for creep damage predictions in finite element (FE) software ABAQUS developed by Dassault systemes, version 2020 [34]. The proposed model can model creep prediction curves precisely covering primary, secondary, and tertiary stages for the grades of stainless steel [35].

2. Theoretical Framework for New Creep Material Model

The new model used a similar approach of integration as used in established models described earlier [36]. It is a well-known fact that the Kachanov–Rabotnov model was initially derived from the Norton–Bailey power law, and the Sine hyperbolic model was derived from McVitty's creep law. Hence, the approach of combining the two models used in this study was realistic. Initially, the creep power laws were used to derive the mathematical formulation by integrating material constants. The Kachanov–Rabotnov model is similar to the Norton–Bailey model except for the introduction of a damage evolution parameter, which predicts the deformation in the tertiary creep stage.

The model was derived using the time-temperature superposition principle (TTP) approach for integrating the Norton–Bailey and Kachanov–Rabotnov models. The approach allows the shifting of experimental data along the time axis by applying an appropriate temperature shift factor [37]. This can be used to obtain creep data at different temperatures, which then can be integrated to obtain a master curve. It is observed that during the primary stage of creep, the creep decelerates due to microstructural changes, such as dislocation, multiplication, and climbing of grains and second-phase precipitation [38]. Therefore, it is crucial to consider the first creep stage for several pure metals and alloys. The Norton–Bailey power law is known to accurately predict primary and secondary creep regimes. The Norton–Bailey creep law is given in Equations (1) and (2).

$$\dot{\varepsilon} = A\,\sigma^n\,t^m, \tag{1}$$

where, $\dot{\varepsilon} = \frac{d\varepsilon_{cr}}{dt}$, $\dot{\varepsilon}$ is the minimum creep strain rate, ε_{cr} is the minimum creep strain, A is the creep parameter, m is material-constant, and n is the stress exponent. They are temperature-dependent material constants that are generally independent of stress. Considering time 't' to be constant for the analysis, Equation (1) is modified to Equation (2) as follows:

$$\dot{\varepsilon} = A\,\sigma^n, \tag{2}$$

There are two techniques for demonstrating the creep deformation and data. The first technique involves keeping the time increments constant and measuring the strain at each point across multiple stresses, known as time hardening. The second technique involves measuring the time it takes to reach set increments of strain called strain hardening. In this research study, a time-hardening technique was applied for modeling the creep data.

The new model used Norton–Bailey law's capability of predicting primary and secondary creep and the Kachanov–Rabotnov damage model ability for the prediction of the tertiary creep regime [39]. The Kachanov–Rabotnov model is given in Equation (3) [40].

$$\dot{\varepsilon} = \frac{d\varepsilon_{cr}}{dt} = A\left(\frac{\sigma}{1-\omega}\right)n, \tag{3}$$

where 'ω' represents the damage evolution variable, which varies from 0 (no damage) to 1 (failure). Equations (1) and (3) were then combined to form the new creep damage model in Equation (4) [41]:

Minimum Creep strain rate:

$$\dot{\varepsilon} = \frac{d\varepsilon_{cr}}{dt} = A\,\sigma^n t^m + A\left(\frac{\sigma}{1-\omega}\right)^n, \tag{4}$$

Solving Equation (4) will yield Equations (5) and (6) as follows:

$$\dot{\varepsilon} = A\,\sigma^n\left[t^m + \frac{1}{(1-\omega)^n}\right], \tag{5}$$

$$\dot{\varepsilon} = A\,\sigma^n\left[\frac{(1-\omega)^n\,t^m + 1}{(1-\omega)^n}\right]. \tag{6}$$

where $\dot{\varepsilon}$ is the minimum creep strain rate and σ is the applied stress. The combined new model was then incorporated into the commercial finite element package ABAQUS using the user subroutine scripting methodology.

Numerical Integration of New Model by Subroutine Scripting

For the subroutine scripting, Equation (6) was converted into numerical form as shown in Equations (7)–(9) [42]:

$$\frac{d\varepsilon}{dt} = \Delta t \overset{Lim}{\rightarrow} 0\ \frac{\Delta\varepsilon}{\Delta t}, \tag{7}$$

$$\frac{\Delta\varepsilon}{\Delta t} = A\,\sigma^n\left[\frac{(1-\omega)^n\,t^m + 1}{(1-\omega)^n}\right], \tag{8}$$

and

$$\Delta\varepsilon = A\,\sigma^n\left[\frac{(1-\omega)^n\,t^m + 1}{(1-\omega)^n}\right]\Delta t \tag{9}$$

where, Δt is the change in time, $\frac{\Delta\varepsilon}{\Delta t}$ is the rate of change in uniaxial deviatoric creep strain increment represented as DECRA(1) in the creep user subroutine [43]. Differentiation of Equation (9) with respect to stress gives Equation (10):

$$\frac{\Delta\varepsilon}{\Delta\sigma} = A\,n\,\sigma^{n-1}\left[\frac{(1-\omega)^n\,t^m + 1}{(1-\omega)^n}\right]\Delta t \tag{10}$$

where $\Delta\varepsilon/\Delta\sigma$, a ratio between the change in strain and the change in stress is termed von Mises stress and represented as DECRA(5) in the creep user subroutine. Equations (9) and (10) can be used in the creep user subroutine to implement the modified creep model in ABAQUS.

3. Methodology

3.1. Incorporating Creep Model in ABAQUS by CREEP User Subroutine Scripting

The flowchart in Figure 1 shows the implementation of the user subroutine script written for the new creep model [44]. The parametric study was carried out to track the material's creep deformation behavior while varying the input creep parameter and stress exponent, which are useful for the model's sensitivity analysis [45].

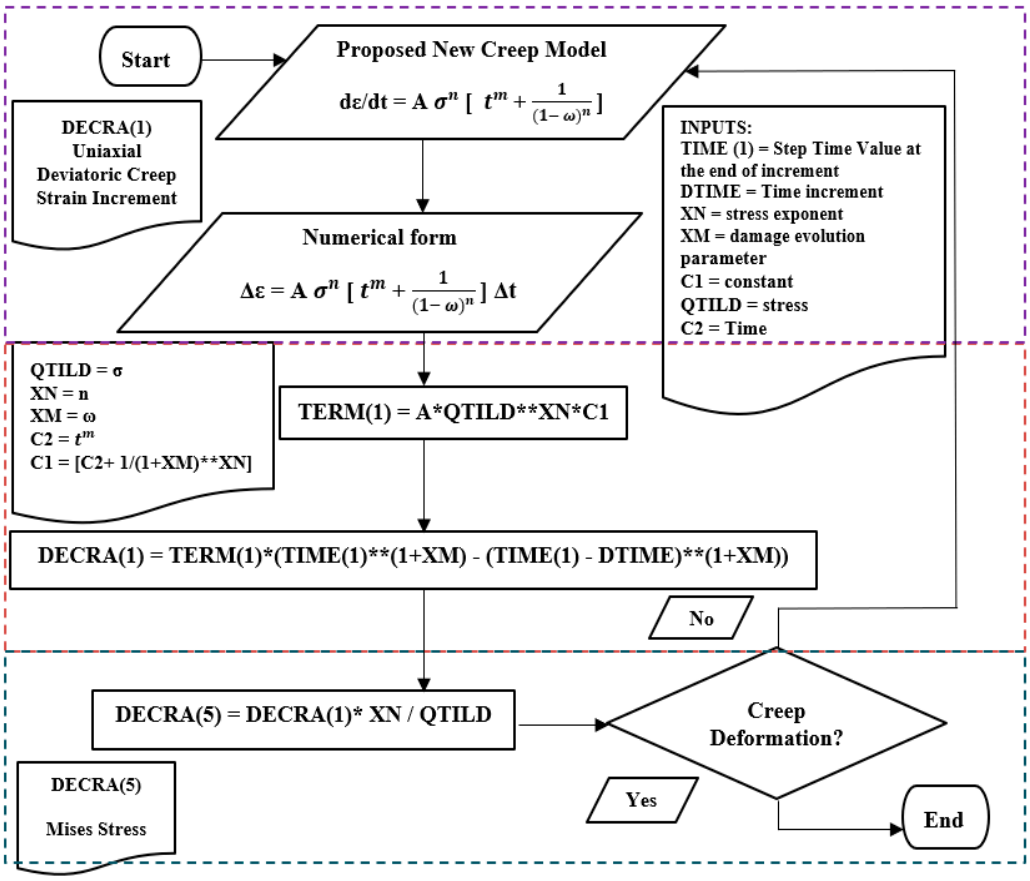

Figure 1. CREEP Subroutine flowchart for the new model. - - - New creep model mathematical formulation flowchart; - - - Uniaxial deviatoric creep strain increment routine flowchart DECRA(1); - - - von Mises stress routine flowchart DECRA(5), *, ** Multiplication signs.

CREEP user subroutine was used to define the material behavior and provide the 'uniaxial' creep laws in a general time-dependent, visco-plastic material formulation [46]. The subroutine was used in couple time-temperature displacement and modified accordingly for the implementation of the new creep model [43].

3.2. Geometry Modeling and Pre-Processing

The dog bone shape specimen geometry was modeled in FE package ABAQUS following ASTM E-139 tensile creep testing standards [47]. The dimensions of the specimen modeled are shown in Figure 2. The boundary conditions in the model were kept consistent with those used in creep experiments. The material behavior under constant elastic stress at room and elevated temperatures was observed, and the geometry model is based on an elastic-perfectly-plastic model in ABAQUS [48]. The plastic hardening data of the material with isotropic material behavior was also obtained for Norton–Bailey, MPC-Omega, and the new model [49]. A uniaxial force was applied on the specimen in the thermal field from one end, keeping the other end fixed. The temperature in the model was kept from 0 to 700 °C for creep visco-plastic thermal material behavior. A kinematic coupling con-

straint was selected for the reference point to apply uniaxial force in the thermal field in a uniform degree of freedom in a global coordinate system [50].

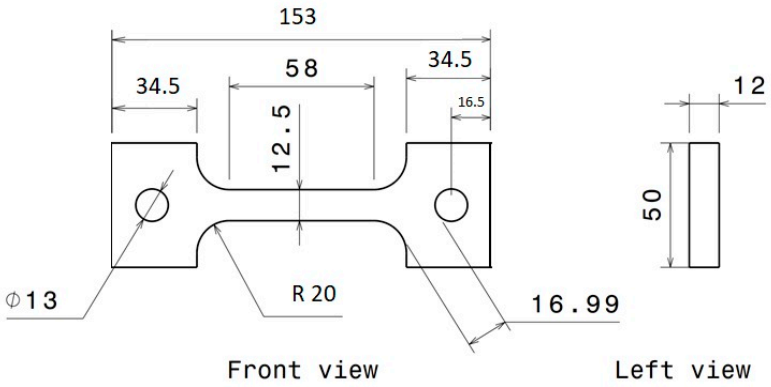

Figure 2. Standard dimensions (in mm) of dog bone specimen [7].

Figure 3a depicts the applied boundary conditions to the specimen, fixed at one end and the load applied at the other end of the specimen. Figure 3b depicts the specimen for thermal analysis as the pre-defined temperature field was defined with the temperature, the step was initial, distribution was direct to specification, instantaneous, and kept constant throughout the region up to 700 °C for running the simulations [51]. Figure 3c illustrates the interaction which was selected as surface-to-surface contact. The coupling constraint was selected for the reference point, and the coupling type was kinematic and with uniform degrees of freedom for the global coordinate system [52].

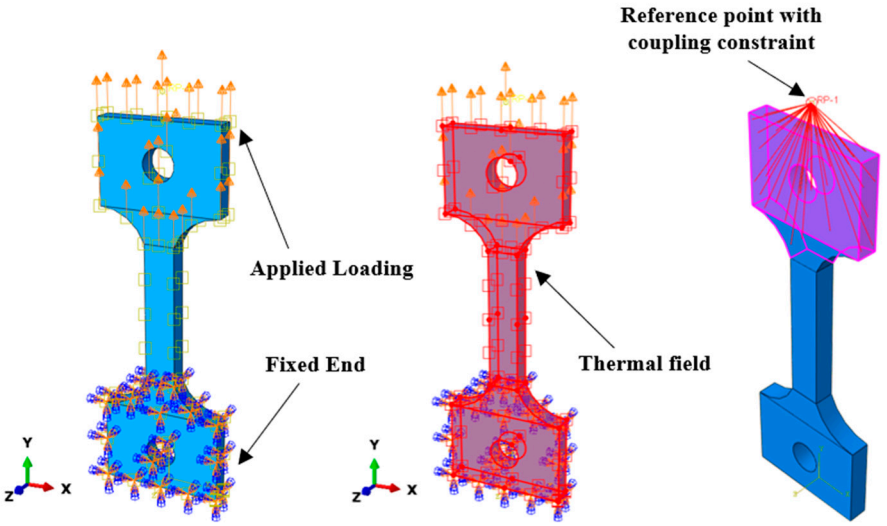

Figure 3. (**a**) SS-304 specimen with pre-defined boundary condition; (**b**) Specimen with thermal field 700 °C and constant throughout the region; and (**c**) Reference point with coupling constraint for the movement of the specimen [7].

The temperature-dependent Young's modulus, plastic strain, and yield stress of the SS-304 material were acquired from ASME BPVC section II part D standards [46] and are shown in Table 1. Density, thermal conductivity, and thermal expansion coefficient values are also taken from the ASME standards. Since all the material properties are extracted from the standards, they are the linear functions of temperature range with no non-linear variations for stainless steel. A decrease in Young's modulus and yield strength of the stainless steel 304 material was observed, corresponding to the increase in temperature while obtaining the properties from the standards.

Table 1. Material and physical properties of SS-304 material [7].

Material Model	Elastic Perfectly Plastic
Young's Modulus	(201,000–17,100) MPa @ −25 °C to 720 °C
Poisson's ratio	0.31
Density	8000 kg/m^3
Thermal Expansion Coefficient	17.3 × 10^{-6} °C^{-1}
Thermal Conductivity	16.2 W m^{-1} °C^{-1}
Yield Stress	(207–126) MPa
Plastic Strain	(0–0.015)

Figure 4 shows the meshed geometry of the FE dog bone specimen with the area of maximum creep deformation highlighted. A mesh convergence study was carried out to obtain the optimum mesh size for the simulations [53]. It was observed that the element mesh size of 3 provided a consistent and concise von Mises stress value of 126 MPa for the specimen. This mesh size resulted in a total of 1700 elements used for meshing the FE geometric model, and the total mesh size for the model is 5100.

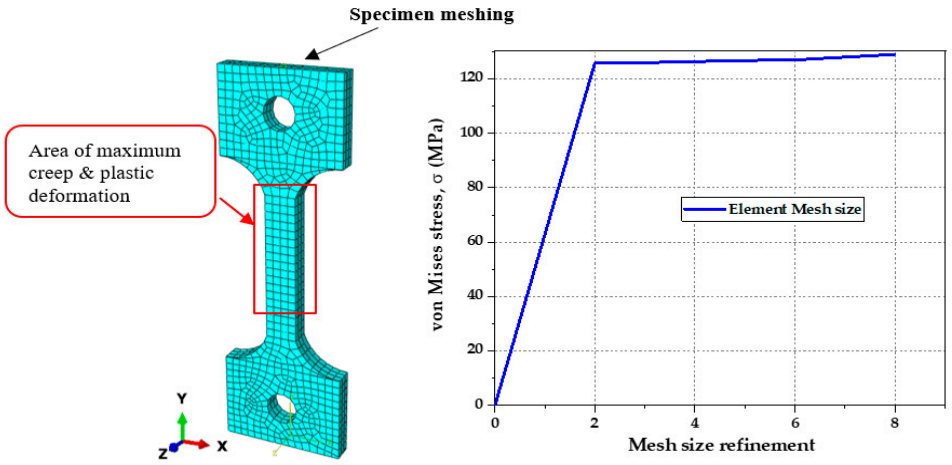

Figure 4. Meshing of FE dog bone model with mesh convergence plot [7].

The creep parameters and stress exponents, which are temperature-dependent material constants and are independent of stresses, were obtained from curve fitting of the baseline Omega model to the new model for damage progression by regression analysis and are shown in Table 2. Tertiary-stage creep and material behavior until rupture were considered in the determination of these values. The results obtained for the new model from the creep subroutine scripting methodology were compared, and the margin of error was analyzed for the method.

Table 2. Material constants for SS-304 for creep models at (680–720) °C.

	Creep Parameters (*A*)	Stress Exponents (*n*)	Temperature (°C)
New Model	1.59818 × 10^{-21}	7.1138481	680
	4.25033 × 10^{-21}	7.0399763	690
	1.10787 × 10^{-20}	6.9676230	700
	2.83197 × 10^{-20}	6.8967418	710
	7.10362 × 10^{-20}	6.827288	720

3.3. Creep Experimental Testing

The creep tests were conducted at 600 °C up to 336 h, and the other laboratory test was conducted at 700 °C up to 1000 h on SS-304 dog bone specimens. The creep specimens were firmly clamped by clevis couplings and then heated to a temperature between 600 °C and 700 °C, surrounded by a thermostatically controlled furnace [54]. The temperature was controlled by a thermocouple attached to the gauge length of the specimen. Once the desired temperature was reached, a constant load of 50 N was applied to exert a longitudinal force on the specimen. During the test, the temperatures, load, and specimen elongation were continuously recorded, and the test continued until the specimen ruptured. The creep curves obtained from the FE analysis were compared with the experimental creep testing data. A regression analysis was conducted to extrapolate the creep data to convert material constants into temperature-dependent functions and to predict the stainless steel 304 material behavior for creep deformation. The creep design maps were plotted by making the extrapolative predictions of creep behavior practical. The creep testing plan for conducting the creep test experiment is exhibited with the help of the flowchart in Figure 5. The experiment tests were conducted on the creep testing machine, as in Figure 6. The specifications of the creep testing machine are tabulated in Table 3, creep testing parameters are tabulated in Table 4, and the testing conditions are tabulated in Table 5.

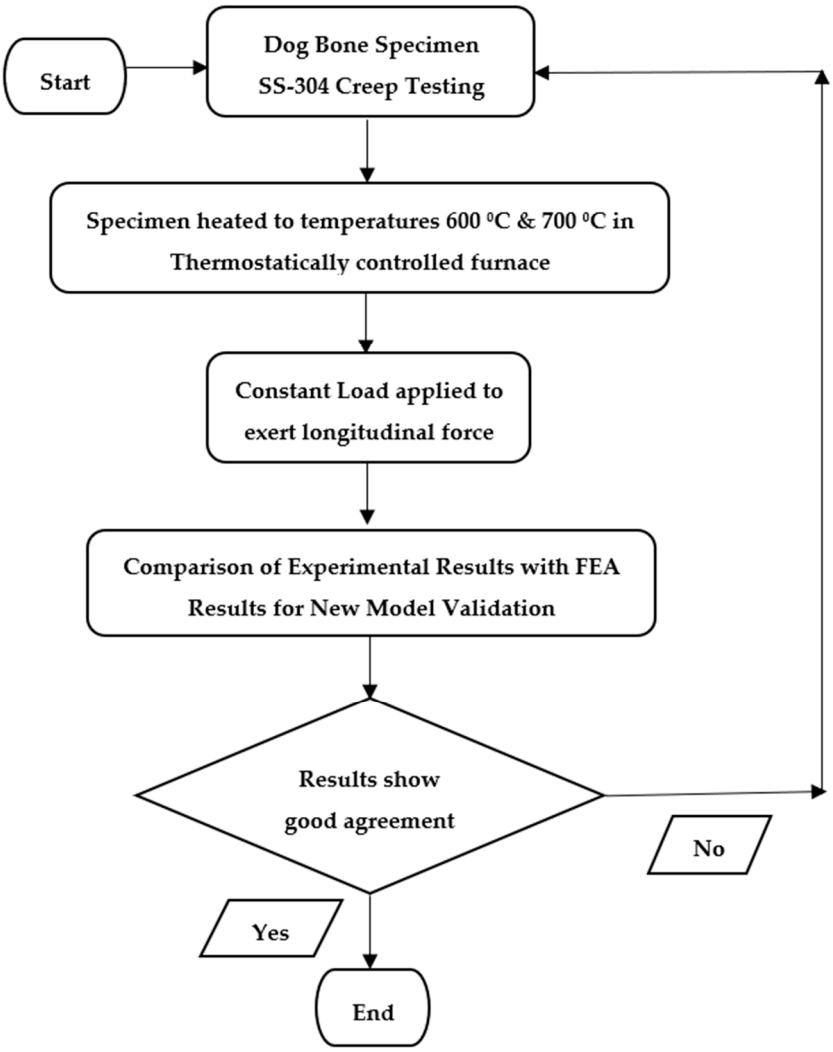

Figure 5. Creep testing plan.

Figure 6. Creep testing machine.

Table 3. Specifications of creep testing machine.

Features	Details
Machine type	Servo control
Capacity	20 tons
Load resolution	1/500,000/+/−0.5%
Test speed	0.001–500 mm/min
Speed accuracy	+/−0.5%
Stroke resolution	0.00003 mm
Computer acquisition frequency	200 times/s or 500 times/s

Table 4. Creep testing parameters.

Parameters	Description			
Material	Stainless Steel-304			
Number of specimens	2 samples			
Stepped Iso-thermal Method (SIM)	Pretension load at 7000 Pa			
	550 °C	600 °C	650 °C	700 °C
Stepped Iso-stress Method (SSM)	Temperature 700 °C			
	5000 Pa	7000 Pa	8000 Pa	10,000 Pa
Preliminary tests Pre-tension Load	6000 Pa	7500 Pa	8000 Pa	8000 Pa
Temperature	600 °C	650 °C	650 °C	700 °C

Table 5. Testing Conditions for Creep Test.

Test Duration (h)	Temperature (°C)	Specimens	Loading Conditions	Yield Strength
336	600	1	74.28 MPa	60%
1000	700	2	52.20 MPa	60%

The influence of continuous load growth factor was continuously monitored by a creep testing machine in the form of specimen deformation. The load growth rate factor used for stainless steel 304 specimen varies as the applied load was different at different temperatures and increased gradually for the stepped iso-thermal and stepped iso-stress methods. The loads are mentioned in Table 4; the load growth rate factor influencing the creep test was recorded for different loading conditions and different temperatures for the stepped iso-stress and iso-thermal methods and for pre-tension loading.

4. Results

The pre-defined boundary conditions were applied in ABAQUS for the dog bone specimen to simulate the creep behavior up to 18,000 h at 720 °C and stress at 126 MPa [55]. The analysis showed promising results covering the primary, secondary, and tertiary stages of creep for the material. The results were obtained by adapting the creep user subroutine scripting method for the new model implementation. Figure 7 shows von Mises and relaxed stress in the SS-304 material obtained from simulation applying the new model and calibrating it with the baseline Omega creep model by regression analysis.

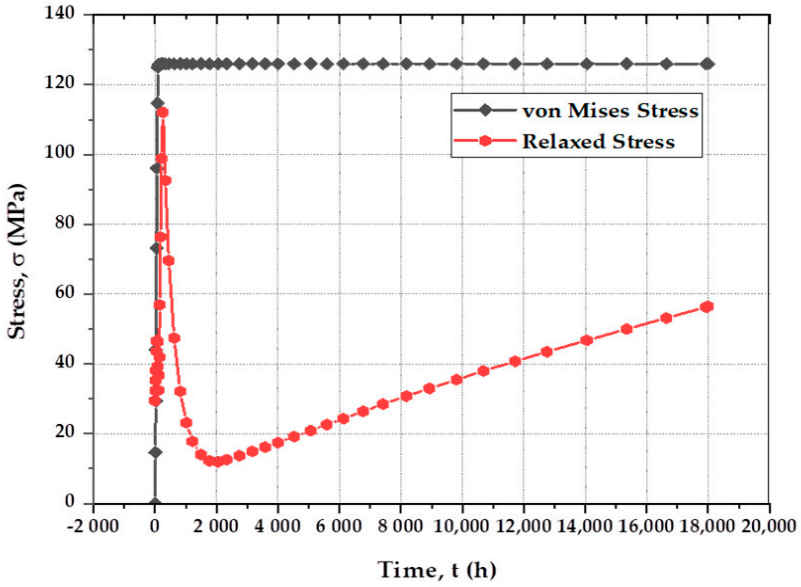

Figure 7. von Mises stress and relaxed stress distribution with Omega-new model's regression visco-elastic plastic run-time of 18,000 h, at 126 MPa and 720 °C.

Figure 8a shows the von Mises stress distribution after 18,000 h of simulation. The significant stresses were created at the free end, whereas the lesser stresses were distributed around the specimen's fixed end. The material began to deform as soon as the continuous load was applied [56]. It transitioned from an elastic to a permanent plastic deformation state under the effect of the temperature environment and specified boundary conditions [49]. For the imposed stresses, Figure 8b,c shows the creep and plastic strains in the specimen, in which the deformation was apparent. Figure 9 depicts the plot of creep strain, plastic strain, and total inelastic strain accumulated with the combination of creep and plastic strain results for the new creep model. Section 4.1 covers the results obtained for the new model by implementing the creep user subroutine method for the new creep model's implementation.

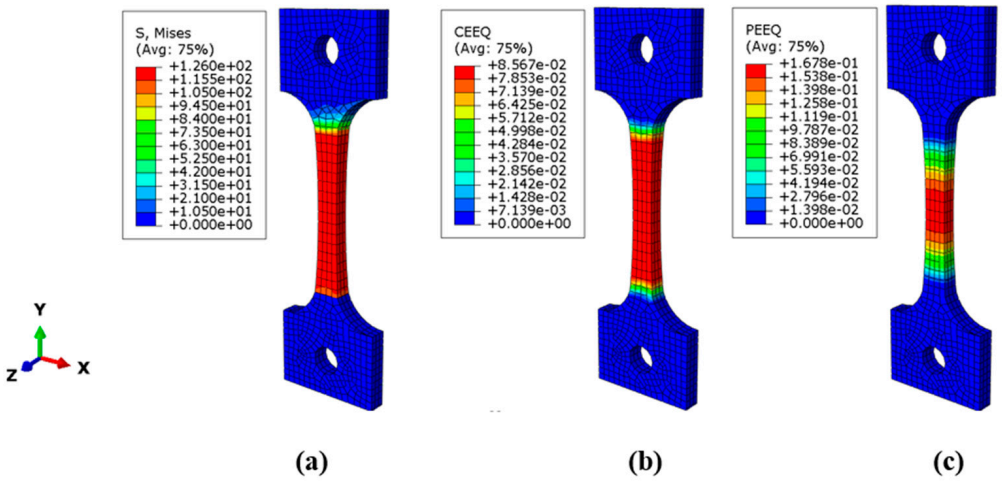

Figure 8. (**a**) Induced von Mises stress in the specimen after running simulations; (**b**) Creep strain (CEEQ) for the applied stresses; and (**c**) Plastic strain (PEEQ) at 720 °C, 18,000 h, and 126 MPa.

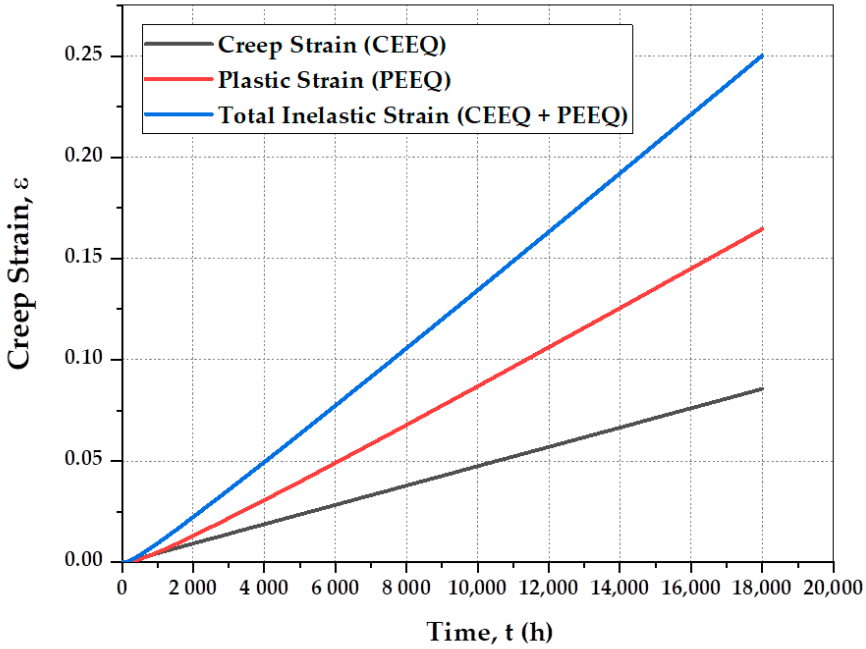

Figure 9. Plastic strain, accumulated creep, and total inelastic strain for SS-304 dog bone specimen by implementing a new creep model.

4.1. New Creep Model Results by User Subroutine Scripting

The CREEP user subroutine available in ABAQUS documentation [43] was modified as depicted in the flowchart of Figure 1. Figure 10 shows the variation in creep strain rate obtained from the new and the established Omega and Norton–Bailey models. Similarly, the graph in Figure 11 represents creep strain for the new model when compared with Omega and Norton–Bailey models at the same pre-defined conditions. The results are evidence of the accuracy of the new model for predicting creep strain rate and creep strain curves in comparison to the Omega and Norton–Bailey models.

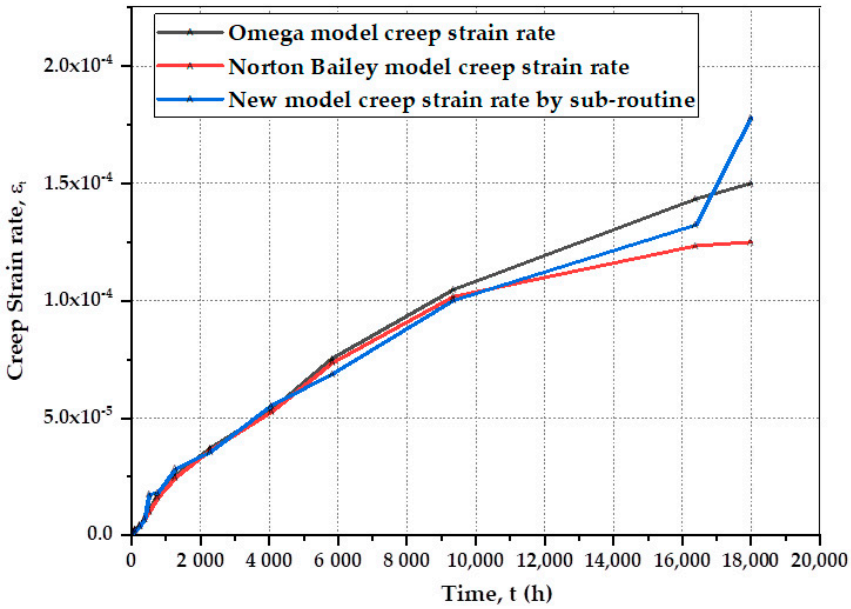

Figure 10. Comparison of creep strain rates between the new, Omega, and Norton–Bailey models by subroutine scripting up to 18,000 h at 720 °C.

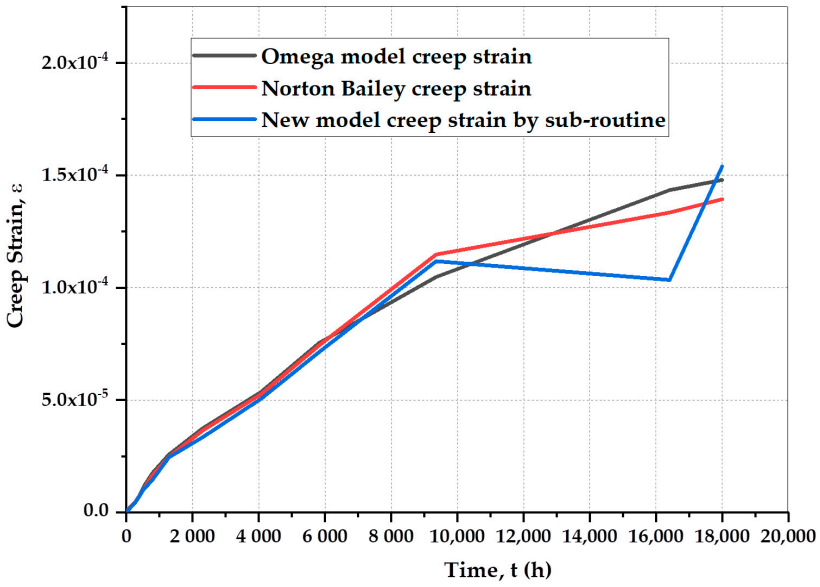

Figure 11. Comparison of creep strains between the new, Omega, and Norton–Bailey model by subroutine scripting up to 18,000 h at 720 °C.

As per the above comparisons and analysis, a good agreement for creep prediction was observed between the results obtained for creep strain rate for the new model using the user subroutine scripting method. The curves showed primary creep deformation for 200 h followed by steady-state secondary creep deformation up to 16,000 h, leading to the sudden creep collapse until rupture for the tertiary creep stage up to 18,000 h. However, the Omega and Norton–Bailey model's curves are unable to model the tertiary stage creep curve. One advantage of the parametric study with the implementation of the subroutine method is that it can be applied to the family of stainless-steel materials to measure the creep deformation behavior of various alloys with similar material characteristics. The variable parameters can be applied to model the materials' behavior at different isotherms at various operating hours, as per experimental testing, to verify the reliability of the new model. It was found that the new model's accuracy was 91.56% by the subroutine method

when compared with the Omega and Norton–Bailey models, with a 5% maximum window of deviation for creep strain rates on ten selected points taken as a reference along the creep strain rate curve. In addition, it was found that the new model's accuracy for creep strain curves was 83.1% by subroutine technique when compared with the Omega and Norton–Bailey models, respectively, with the same 5% empirical deviation. Again, there was good agreement in the results found for the analysis of the creep damage prediction. Therefore, the method can be applied for the creep prediction simulations for stainless steel using the newly developed model.

To capture the tertiary creep behavior of stainless-steel material, various damage evolution parameter (ω) values were applied. The creep strain to reach the particular values of (ω) does not show a similar trend. The creep strain curves at different values of (ω) proved the evidence of nonlinear material behavior. As depicted in Figure 12, a marginal decrease in strain to reach the value of (ω) resulted in lower applied stresses. The kinetics evolution of coupled strain and damage does not necessarily follow the same trend. It is well known and proven that any material would fail if ω reaches the critical damage ω_{cr} value of 1. The material usually fails and deforms before reaching the critical damage (ω_{cr}) equivalent to 1 [57].

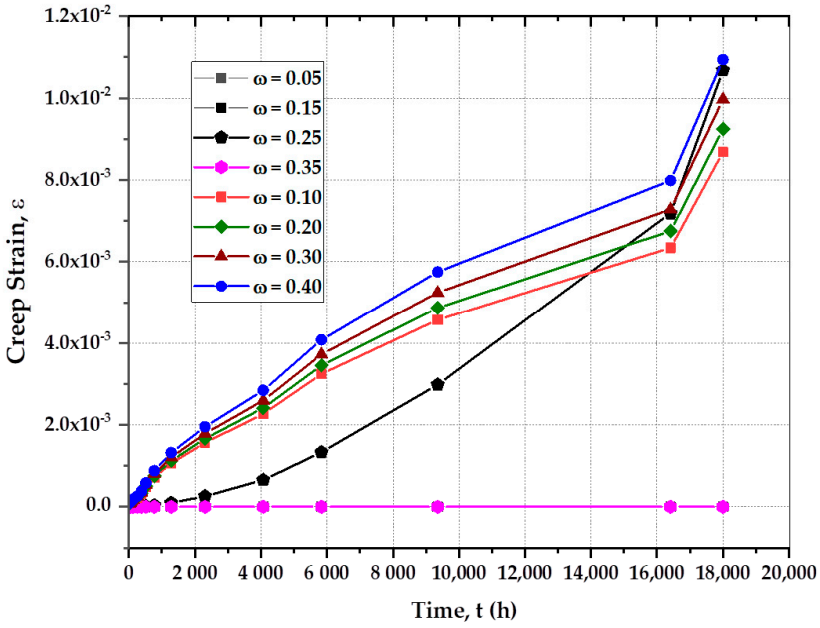

Figure 12. Creep strain for the new model at varying damage evolution parameters up to 18,000 h [58].

The results show good agreement for the creep strain rate obtained for varying stresses at elevated temperatures. The adapted method of subroutine scripting can be implemented to model the creep deformation behavior of SS-304 material for defined boundary conditions and at elevated temperatures [59]. The increase in stress would result in the rise of creep strain rate and creep strain. The curves at different temperatures are clearly exhibited for the primary, secondary, and tertiary creep stages of the SS-304 material.

4.2. Experimental Creep Test Results

A series of experimental tests were conducted as per ASTM standards [53]. A total of 11 specimens were used. Nine samples were used for tensile tests, and two tests were used for the creep tests. Ambient tests were conducted on three samples to verify the yield strength of SS-304, whereas hot tensile tests were conducted on the next six samples; three samples at 600 °C and the remaining three at 700 °C, in order to verify the ultimate tensile strength at elevated temperature prior to the creep tests.

The creep specimens were subjected to pre-load for 336 h and 1000 h. During the test, the specimens' deformations were recorded to estimate the primary, secondary, and

tertiary stages of creep phenomena. High material degradation was observed by the deformed microstructure examinations of grain distortion, elongation, and grain boundary sliding [58]. Plots in Figure 13 indicate the creep curves obtained for both testing conditions of SS-304 specimens at 336 h and 1000 h, respectively.

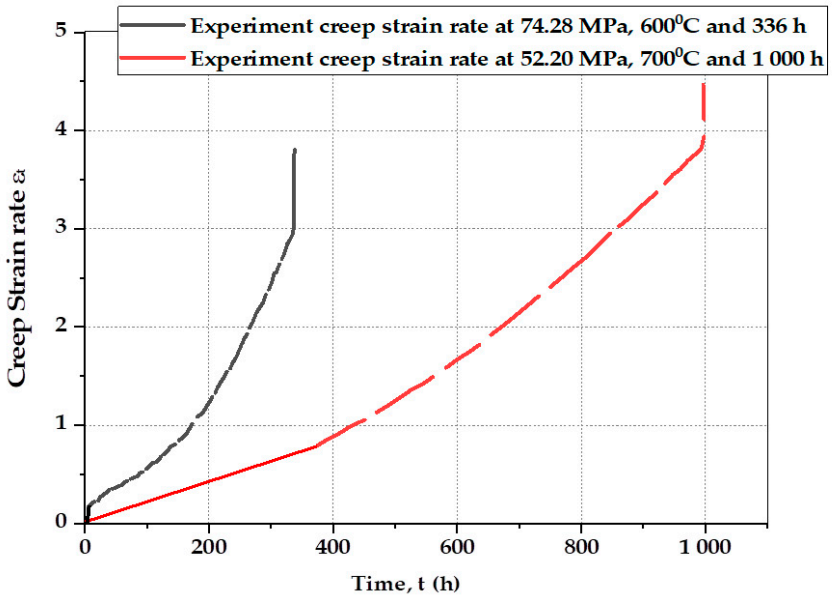

Figure 13. Creep curves for 336 h creep test with loading conditions 60% yield strength (74.28 MPa) at 600 °C and 1000 h creep test with loading conditions 60% yield strength (52.20 MPa) at 700 °C.

4.3. New Creep Model Validation with Creep Experimental Results

Figure 14 depicts the comparison of creep strain rate curves obtained through the 1000 h creep test with those obtained by FE simulation for the same conditions, using the newly proposed creep model simulated using the user subroutine technique. Similarly, Figure 15 depicts the creep strain rate curves obtained from creep experiments up to 336 h and compared with the new creep model [60].

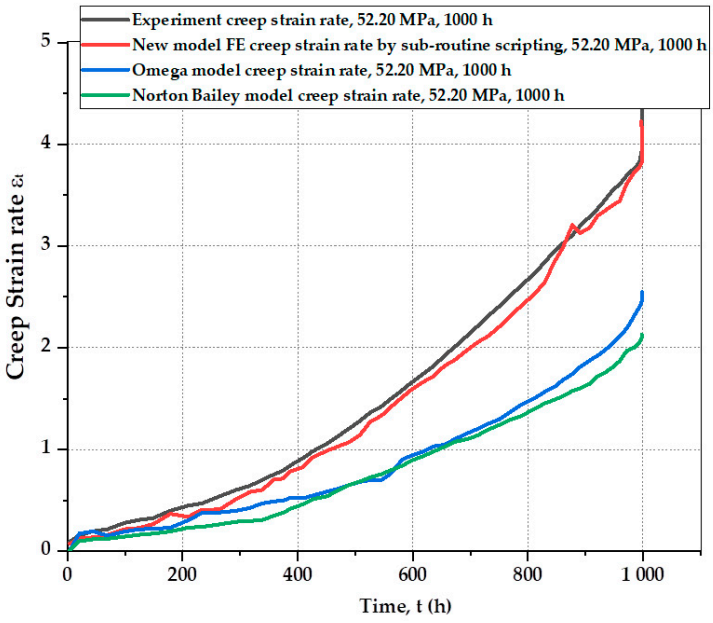

Figure 14. Comparison of predicted creep strain rate by the new creep model using the user subroutine method with experiment creep strain rate at 700 °C and 1000 h.

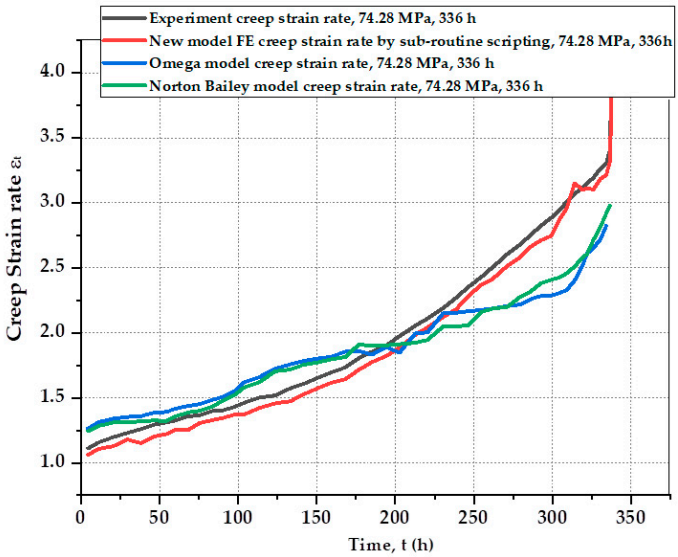

Figure 15. Comparison of predicted creep strain rate by the new creep model using the user subroutine method with experiment creep strain rate at 600 °C and 336 h.

It is calculated that the results of creep strain rate by user subroutine scripting method are 90.69% near accurate to the actual experimental creep test results of 1000 h. Similarly, for the comparison with the experimental results at 336 h, the creep strain rates from the simulation indicated a comparable accuracy of 92.66%, using the subroutine scripting method for model implementation. The percentage accuracy is based on the creep data and is calculated by considering 10 points on the experimental creep curve with a 5% maximum deviation. Hence, the proposed new model is validated with the help of laboratory creep test results [61]. The validation is mandatory to prove the relevance of the proposed creep model applied to various materials and equipment exposed to different service conditions. The peak in the creep strain rate curve was observed while running the simulations for the 336 h creep test and was recorded [62].

It is evident that the new creep model has the capability to predict the creep deformation for stainless steel material more accurately in comparison to other models at elevated temperatures. The new creep model successfully simulated the creep curve, starting with the instantaneous elongation of the primary creep stage up to 300 h, followed by the steady-state secondary creep deformation up to 16,000 h and then rapid distortion until rupture for the tertiary creep stage up to 18,000 h.

4.4. Results Comparison of New Creep Model with the Existing Models

The following graphs in Figure 16a depict the comparison specifically between the new model and the other models, established by performing the simulations on the same physical conditions and applying the creep models simultaneously for creep strain rates. The new model and the established models were calibrated with the Omega model in order to extract stress exponents and creep parameters [63].

Similar comparisons are being made for creep strains at the same physical conditions that indicated promising results. The results proved the capability of the new creep model in modeling all three creep stages for SS-304 material at elevated temperatures. Figure 16b shows the results for the creep strains of the new model when compared with the established models for the same physical conditions while running the simulations for up to 18,000 h, 126 MPa, and 720 °C [64].

The damage is apparent at the tertiary stage of creep damage, which was recorded in the following graph by plotting the damage evolution parameter against creep strains as in Figure 17. The comparisons were made for creep strain between established models and the new proposed model to justify the results. The increase in creep strain result observed

was due to the rise of the damage evolution parameter to model the tertiary creep curve with the damage progression.

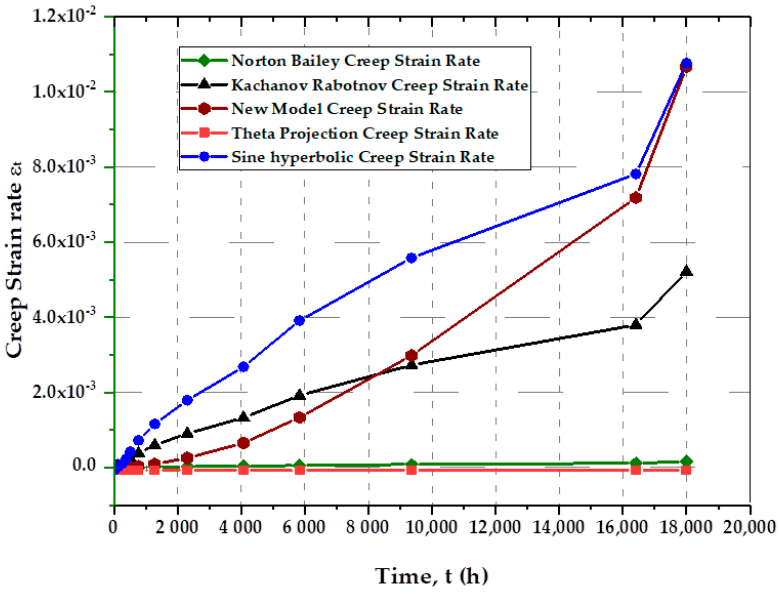

(**a**)

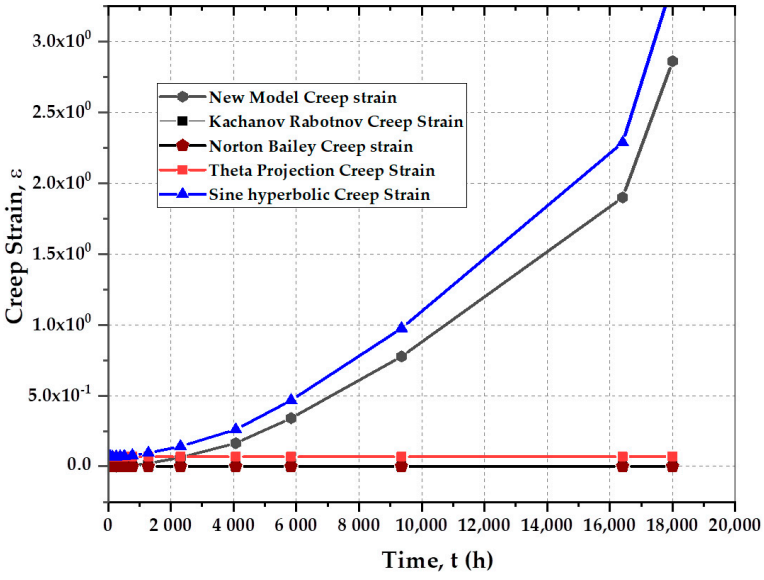

(**b**)

Figure 16. (**a**) Comparison of the new model with established models for creep strain rate at 720 °C and 126 MPa; (**b**) Comparison between the new model and established models for creep strain at 720 °C and 126 MPa.

For the case studies, a modified theta projection model was applied to ferritic steel alloy 2.25Cr–1Mo to characterize its creep behavior at an elevated temperature of 754 °C [65]. Similarly, the new proposed model is applied to the same material, whose material and physical properties were obtained from the ASME BPVC, sub-part II, section D standards. By considering the same FE dog bone model with the same geometry and running the FE simulations at similar conditions of 754 °C, 110 MPa, and up to 300 h, it was found that the new model's accuracy was 88.5%, and the modified theta projection model accuracy was 84.3% when compared with the published experimental creep test data. For the other

case study, a Sine hyperbolic model was applied to predict the creep curve for ferritic steel 2.25Cr–1Mo at 90 MPa, 750 °C, and the test ran for up to 1000 h [66]. The new model was applied to the same material, and the same conditions were maintained. The new model's precision was 92%, and the Sine hyperbolic model's accuracy was 82% when compared with the published experimental creep test data. Hence, the significance and relevance of the new model is proved [67].

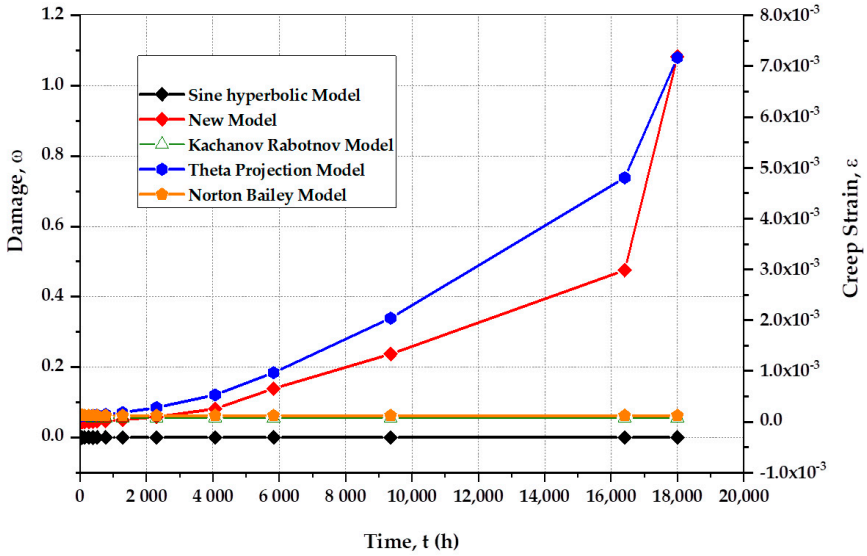

Figure 17. Comparison of creep strain and damage evolution parameters between the new model and established models at 720 °C and 126 MPa.

5. Conclusions

The integration of the Kachanov–Rabotnov and Norton–Bailey models into the new material model has provided a new approach to creep modeling. The model was integrated into the ABAQUS software using the subroutine scripting methodology, which allowed for the accurate prediction of creep behavior under various loading conditions. The following conclusions can be deduced from the research study:

- When compared with Omega and Norton–Bailey models, the model's accuracy in predicting the creep strain rates was found to be 91.56% by subroutine scripting. Similarly, for the creep strain, the results indicated accuracies of 83.1% by the same method of writing subroutine while comparing with the Omega and Norton–Bailey models.
- The validation of the new model was performed by comparing the results between finite element and experiment creep tests carried out up to 336 h and 1000 h. The results of creep strain rate by subroutine scripting are 90.69% near accurate and close to the 1000 h experimental creep test results.
- Similarly, for the comparison with the experimental results at 336 h, the creep strain rates from the simulation indicated a comparable accuracy of 92.66%, using the subroutine scripting method.
- The new model, when applied to a couple of case studies, fetched more precise results in comparison to the established models. The model accuracy was 88.5%, and the modified theta projection model accuracy was 84.3% when applied to the material 2.25Cr–1Mo under the same conditions and compared with the published experiment creep test results. Similarly, the new model's accuracy was 92% in comparison to the Sine hyperbolic model's accuracy of 82%, when compared with the published experiment test data for the material 2.25Cr–1Mo under the same conditions.

Further investigations into the application of this model for other materials and loading conditions are needed to validate its applicability. However, the successful validation of the model against experimental data suggests that it has a promising future and will be useful in a wide range of engineering applications.

Author Contributions: M.S.—Literature search, writing, editing, data analysis, figures, data collection; A.R.O.—manuscript review, supervision, funding acquisition, resources; M.F.O.—manuscript editing, software, data interpretation, review; H.T.A.—funding acquisition, data analysis, study design, editing; M.K.K.—study design, writing, editing, review, data analysis. All authors have read and agreed to the published version of the manuscript.

Funding: The research work was funded by the Deanship of Scientific Research at Taif University, Kingdom of Saudi Arabia and PETRONAS, Malaysia Industrial Grant; Grant No: 015MD0-156.

Data Availability Statement: The data presented in this research study are available on request.

Acknowledgments: The authors would like to acknowledge the financial support through Deanship of Scientific Research at Taif University, Kingdom of Saudi Arabia and technical support through Digital Analytics Structural Integrity Technology Group (DASIT), Universiti Teknologi PETRONAS, Malaysia which are greatly appreciated.

Conflicts of Interest: The authors declare no conflict of interest.

Nomenclature

A	Norton's power-law constant
n	Stress exponent
tr	Rupture time
σ1, σ2, and σ3	Principal stresses
S1	Stress parameter
α	Triaxiality parameter
ω	Omega damage parameter
δ_Ω	Omega parameter
ε_0	Initial creep strain
Ω	Omega material damage constant
ε_t	Creep strain rate
FFS	Fitness for service
API	American Petroleum Institute
UTS	Ultimate tensile strength
MPC	Material Properties Council
ASME	American Society for Mechanical Engineers
BPVC	Boiler and pressure vessel codes
UTS	Ultimate tensile strength
ASTM	American Standards for Testing of Materials
CDM	Continuum damage mechanics
KR	Kachanov–Rabotnov model
NB	Norton–Bailey Model
TP	Theta Projection model
SH	Sine-hyperbolic model

References

1. Yao, H.-T.; Xuan, F.-Z.; Wang, Z.; Tu, S.-T. A review of creep analysis and design under multi-axial stress states. *Nucl. Eng. Des.* **2007**, *237*, 1969–1986. [CrossRef]
2. Wu, X.; Williams, S.; Gong, D. A True-Stress Creep Model Based on Deformation Mechanisms for Polycrystalline Materials. *J. Mater. Eng. Perform.* **2012**, *21*, 2255–2262. [CrossRef]
3. Salam, I.; Tauqir, A.; Khan, A. Creep-fatigue failure of an aero engine turbine blades. *Eng. Fail. Anal.* **2002**, *9*, 335–347. [CrossRef]
4. Yukalov, V.I. Saga of Superfluid Solids. *Physics* **2020**, *2*, 49–66. [CrossRef]
5. Benaarbia, A.; Xu, X.; Sun, W.; Becker, A.; Jepson, M.A. Investigation of short-term creep deformation mechanisms in MarBN steel at elevated temperatures. *Mater. Sci. Eng. A* **2018**, *734*, 491–505. [CrossRef]
6. You, D.; Michelic, S.K.; Presoly, P.; Liu, J.; Bernhard, C. Modeling Inclusion Formation during Solidification of Steel: A Review. *Metals* **2017**, *7*, 460. [CrossRef]
7. Jaffré, K.; Ter-Ovanessian, B.; Abe, H.; Mary, N.; Normand, B.; Watanabe, Y. Effect of Mechanical Surface Treatments on the Surface State and Passive Behavior of 304L Stainless Steel. *Metals* **2021**, *11*, 135. [CrossRef]
8. Penny, R.; Weber, M. Robust methods of life assessment during creep. *Int. J. Press. Vessel. Pip.* **1992**, *50*, 109–131. [CrossRef]

9. Haque, M.S.; Stewart, C.M. The disparate data problem: The calibration of creep laws across test type and stress, temperature, and time scales. *Theor. Appl. Fract. Mech.* **2019**, *100*, 251–268. [CrossRef]
10. Sattar, M.; Othman, A.R.; Muzamil, M.; Kamaruddin, S.; Akhtar, M.; Khan, R. Correlation Analysis of Established Creep Failure Models through Computational Modelling for SS-304 Material. *Metals* **2023**, *13*, 197. [CrossRef]
11. Sattar, M.; Othman, A.; Kamaruddin, S.; Akhtar, M.; Khan, R. Limitations on the computational analysis of creep failure models: A review. *Eng. Fail. Anal.* **2022**, *134*, 105968. [CrossRef]
12. Bråthe, L.; Josefson, L. Estimation of Norton-Bailey parameters from creep rupture data. *Met. Sci.* **1979**, *13*, 660–664. [CrossRef]
13. Golan, O.; Arbel, A.; Eliezer, D.; Moreno, D. The applicability of Norton's creep power law and its modified version to a single-crystal superalloy type CMSX-2. *Mater. Sci. Eng. A* **1996**, *216*, 125–130. [CrossRef]
14. May, D.L.; Gordon, A.P.; Segletes, D.S. The Application of the Norton-Bailey Law for Creep Prediction through Power Law Regression. In Proceedings of the ASME Turbo Expo, San Antonio, TX, USA, 3–7 June 2013; Volume 7A, pp. 1–8. [CrossRef]
15. Batsoulas, N.D. Mathematical description of the mechanical behaviour of metallic materials under creep conditions. *J. Mater. Sci.* **1997**, *32*, 2511–2527. [CrossRef]
16. ASME. *American Petroleum Institute API-579, Fitness for Service, Operation Manual*, 3rd ed.; no. FFS-1; The American Society of Mechanical Engineers: Washington, DC, USA, 2016.
17. Prager, M. Development of the MPC Omega Method for Life Assessment in the Creep Range. *J. Press. Vessel. Technol.* **1995**, *117*, 95–103. [CrossRef]
18. Chen, H.; Zhu, G.; Gong, J. Creep Life Prediction for P91/12Cr1MoV Dissimilar Joint Based on the Omega Method. *Procedia Eng.* **2015**, *130*, 1143–1147. [CrossRef]
19. Kachanov, L.M. Rupture Time Under Creep Conditions. *Int. J. Fract.* **1999**, *97*, 11–18. [CrossRef]
20. Stewart, C.M.; Gordon, A.P. Methods to Determine The Critical Damage Criterion of the Kachanov-Rabotnov Law. In Proceedings of the ASME 2012 International Mechanical Engineering Congress and Exposition, Houston, TX, USA, 9–15 November 2012; Volume 3, pp. 663–670. [CrossRef]
21. Lemaitre, J. How to use damage mechanics. *Nucl. Eng. Des.* **1984**, *80*, 233–245. [CrossRef]
22. Harrison, W.J.; Evans, P.W.J. Application of the Theta Projection Method to Creep Modelling Using Abaqus. In *Abaqus Regional Users Conference*; Swansea University: Swansea, UK, 2007; pp. 1–15.
23. Haque, M.S. An Improved Sin-Hyperbolic Constitutive Model for Creep Deformation and Damage. 2015, p. 84. Available online: http://me.utep.edu/cmstewart/documents/MSH_MSME_2015.pdf (accessed on 1 January 2015).
24. Woodford, D.A. Accelerated high temperature performance evaluation for alloy optimization, embrittlement, and life assessment. In Proceedings of the CORROSION 2005, Houston, TX, USA, 3–7 April 2005; Volume 2005.
25. Kim, M.-S.; Kim, H.-T.; Choi, Y.-H.; Kim, J.-H.; Kim, S.-K.; Lee, J.-M. A New Computational Method for Predicting Ductile Failure of 304L Stainless Steel. *Metals* **2022**, *12*, 1309. [CrossRef]
26. Sattar, M.; Othman, A.R.; Akhtar, M.; Kamaruddin, S.; Khan, R.; Masood, F.; Alam, M.A.; Azeem, M.; Mohsin, S. Curve Fitting for Damage Evolution through Regression Analysis for the Kachanov–Rabotnov Model to the Norton–Bailey Creep Law of SS-316 Material. *Materials* **2021**, *14*, 5518. [CrossRef]
27. Zhang, J.; Li, J.; Zan, J.; Guo, Z.; Liu, K. A Creep Constitutive Model, Based on Deformation Mechanisms and Its Application to Creep Crack Growth. *Metals* **2022**, *12*, 2179. [CrossRef]
28. He, J.; Chen, F.; Wang, B.; Zhu, L.B. A modified Johnson-Cook model for 10%Cr steel at elevated temperatures and a wide range of strain rates. *Mater. Sci. Eng. A* **2018**, *715*, 1–9. [CrossRef]
29. Allen, C.; Coules, H.; Truman, C. Investigation into the Effects of Prior Plasticity on Creep Accumulation in 316H Stainless Steel. *Phys. Sci. Forum* **2022**, *4*, 16. [CrossRef]
30. Zhang, L.; Feng, X.; Wang, X.; Liu, C. On the Constitutive Model of Nitrogen-Containing Austenitic Stainless Steel 316LN at Elevated Temperature. *PLoS ONE* **2014**, *9*, e102687. [CrossRef] [PubMed]
31. Koric, S.; Thomas, B.G.; Voller, V.R. Enhanced Latent Heat Method to Incorporate Superheat Effects into Fixed-Grid Multiphysics Simulations. *Numer. Heat Transfer. Part B Fundam.* **2010**, *57*, 396–413. [CrossRef]
32. Koric, S.; Thomas, B.G. Thermo-mechanical models of steel solidification based on two elastic visco-plastic constitutive laws. *J. Mater. Process. Technol.* **2008**, *197*, 408–418. [CrossRef]
33. Zappulla, M.L.; Cho, S.-M.; Koric, S.; Lee, H.-J.; Kim, S.-H.; Thomas, B.G. Multiphysics modeling of continuous casting of stainless steel. *J. Am. Acad. Dermatol.* **2019**, *278*, 116469. [CrossRef]
34. Safari, A.; Forouzan, M.; Shamanian, M. Thermo-viscoplastic constitutive equation of austenitic stainless steel 310s. *Comput. Mater. Sci.* **2013**, *68*, 402–407. [CrossRef]
35. Saeidi, N.; Raeissi, M.; Vaghei, H.; Abdar, M. Extraordinary strength and ductility obtained in transformation-induced plasticity steel by slightly modifying its chemical composition. *Mater. Sci. Eng. A* **2017**, *702*, 225–231. [CrossRef]
36. Srivastava, A.; Ghassemi-Armaki, H.; Sung, H.; Chen, P.; Kumar, S.; Bower, A.F. Micromechanics of plastic deformation and phase transformation in a three-phase TRIP-assisted advanced high strength steel: Experiments and modeling. *J. Mech. Phys. Solids* **2015**, *78*, 46–69. [CrossRef]
37. Staroselsky, A.; Cassenti, B.N. Combined rate-independent plasticity and creep model for single crystal. *Mech. Mater.* **2010**, *42*, 945–959. [CrossRef]

38. Hyde, T.H.; Sun, W.; A Williams, J. Creep analysis of pressurized circumferential pipe weldments—A review. *J. Strain Anal. Eng. Des.* **2003**, *38*, 1–27. [CrossRef]
39. Stewart, C.M.; Gordon, A.P. Strain and Damage-Based Analytical Methods to Determine the Kachanov–Rabotnov Tertiary Creep-Damage Constants. *Int. J. Damage Mech.* **2011**, *21*, 1186–1201. [CrossRef]
40. Stewart, C.M.; Gordon, A.P. Constitutive Modeling of Multistage Creep Damage in Isotropic and Transversely Isotropic Alloys with Elastic Damage. *J. Press. Vessel. Technol.* **2012**, *134*, 041401. [CrossRef]
41. Stewart, C.M. *A Hybrid Constitutive Model for Creep, Fatigue, and Creep-Fatigue Damage*; University of Central Florida: Orlando, FL, USA, 2013.
42. Chang, Y.; Xu, H. The Damage Development and Failure Description Under Multiaxial Creep. In Proceedings of the ASME 2014 Pressure Vessels and Piping Conference, Anaheim, CA, USA, 20–24 July 2014; pp. 1–6.
43. *ABAQUS*, Version 6.12. User's Documentation 3.4.6. Dassault Systèmes: Waltham, MA, USA, 2013; Volume IV.
44. Sarkar, S.; Singh, I.; Mishra, B.; Shedbale, A.; Poh, L. Source codes and simulation data for the finite element implementation of the conventional and localizing gradient damage methods in ABAQUS. *Data Brief* **2019**, *26*, 104533. [CrossRef] [PubMed]
45. Abdallah, Z.; Gray, V.; Whittaker, M.; Perkins, K. A Critical Analysis of the Conventionally Employed Creep Lifing Methods. *Materials* **2014**, *7*, 3371–3398. [CrossRef]
46. Qi, W.; Brocks, W.; Bertram, A. An FE-analysis of anisotropic creep damage and deformation in the single crystal SRR99 under multiaxial loads. *Comput. Mater. Sci.* **2000**, *19*, 292–297. [CrossRef]
47. Al-Bakri, A.A.; Sajuri, Z.; Ariffin, A.K.; Razzaq, M.A.; Fafmin, M.S. Tensile and Fracture Behavior of very thin 304 Stainless Steel Sheet. *J. Teknol.* **2016**, *78*, 45–50. [CrossRef]
48. Jones, D.P.; Gordon, J.L.; Hutula, D.N.; Banas, D.; Newman, J.B. An Elastic-Perfectly Plastic Flow Model for Finite Element Analysis of Perforated Materials. *J. Press. Vessel. Technol.* **2000**, *123*, 265–270. [CrossRef]
49. González-Gómez, P.; Gómez-Hernández, J.; Briongos, J.; Santana, D. Lifetime analysis of the steam generator of a solar tower plant. *Appl. Therm. Eng.* **2019**, *159*, 113805. [CrossRef]
50. Gupta, A.K.; Anirudh, V.; Singh, S.K. Constitutive models to predict flow stress in Austenitic Stainless Steel 316 at elevated temperatures. *Mater. Des.* **2012**, *43*, 410–418. [CrossRef]
51. Sainath, K. Heat transfer and Thermal Stress Analysis in Internal Grooved tube in comparison with bare tube by Finite element method. *Int. J. Curr. Eng. Technol.* **2010**, *2*, 402–406. [CrossRef]
52. Powers, L.M.; Arnold, S.M.; Baranski, A. Using ABAQUS Scripting Interface for Materials Evaluation and Life Prediction. In Proceedings of the 2006 ABAQUS Users' Conference, Cambridge, MA, USA, 1 January 2006; pp. 1–11.
53. Alemayehu, D.B.; Huang, S.-J.; Koricho, E.G. Experimental and FEM analysis of three carbon steel characterization under quasi-static strain rate for bumper beam application. *MATEC Web Conf.* **2017**, *123*, 00019. [CrossRef]
54. Hu, M.; Li, K.; Li, S.; Cai, Z.; Pan, J. Stress relief investigation using creep model considering back stress in welded rotor. *J. Constr. Steel Res.* **2020**, *169*, 106017. [CrossRef]
55. Galles, D.; A Monroe, C.; Beckermann, C. Measurement and simulation of deformation and stresses in steel casting. *IOP Conf. Ser. Mater. Sci. Eng.* **2012**, *33*, 012049. [CrossRef]
56. Rice, J.R.; Tracey, D.M. On the ductile enlargement of voids in triaxial stress fields. *J. Mech. Phys. Solids* **1969**, *17*, 201–217. [CrossRef]
57. Paso, E.; Ramirez, C.; Paso, E.; Stewart, C.M. A Novel Metamodeling Approach for Time-Temperature Parameter Models. In Proceedings of the ASME 2017 Pressure Vessels and Piping Conference, Waikoloa, HI, USA, 16–20 July 2017; pp. 1–10.
58. Esposito, L.; Bonora, N. Time-independent formulation for creep damage modeling in metals based on void and crack evolution. *Mater. Sci. Eng. A* **2009**, *510–511*, 207–213. [CrossRef]
59. Stewart, C.M.; Gordon, A.P.; Hogan, E.A.; Saxena, A. Characterization of the Creep Deformation and Rupture Behavior of DS GTD-111 Using the Kachanov–Rabotnov Constitutive Model. *J. Eng. Mater. Technol.* **2011**, *133*, 021013. [CrossRef]
60. Hu, M.; Li, K.; Li, S.; Cai, Z.; Pan, J. Analytical Model to Compare and Select Creep Constitutive Equation for Stress Relief Investigation during Heat Treatment in Ferritic Welded Structure. *Metals* **2020**, *10*, 688. [CrossRef]
61. Haque, M.S.; Stewart, C.M. Metamodeling Time-Temperature Creep Parameters. *J. Press. Vessel. Technol.* **2020**, *142*, 031504. [CrossRef]
62. Azizi, G.; Thomas, B.G.; Zaeem, M.A. Prediction of Thermal Distortion during Steel Solidification. *Metals* **2022**, *12*, 1807. [CrossRef]
63. Haque, M.S.; Stewart, C.M. Comparative analysis of the sin-hyperbolic and Kachanov–Rabotnov creep-damage models. *Int. J. Press. Vessel. Pip.* **2019**, *171*, 1–9. [CrossRef]
64. Evans, M. A comparative assessment of creep property predictions for a 1CrMoV rotor steel using the CRISPEN, CDM, Omega and Theta projection techniques. *J. Mater. Sci.* **2004**, *39*, 2053–2071. [CrossRef]
65. Alipour, R.; Nejad, A.F. Creep behaviour characterisation of a ferritic steel alloy based on the modified theta-projection data at an elevated temperature. *Int. J. Mater. Res.* **2016**, *107*, 406–412. [CrossRef]

66. Alipour, R.; Nejad, A.F.; Dezfouli, H.N. Steady State Creep Characteristics of a Ferritic Steel at Elevated Temperature: An Experimental and Numerical Study. *ADMT J.* **2018**, *11*, 115–129.
67. Huespe, A.; Cardona, A.; Nigro, N.; Fachinotti, V. Visco-plastic constitutive models of steel at high temperature. *J. Mater. Process. Technol.* **2000**, *102*, 143–152. [CrossRef]